Journal of Contaminant Hydrology 283 (2026) 105052

Contents lists available at ScienceDirect

Journal of Contaminant Hydrology

journal homepage: www.elsevier.com/locate/jconhyd

Synergistic amplification and threshold vulnerability of coastal aquifer barriers under sea-level rise and freshwater decline

Rajagopal Sadhasivam [a], Venkatraman Srinivasan [a,b,*]

[a] Department of Civil Engineering, Indian Institute of Technology Madras, Chennai, India
[b] School of Sustainability, Indian Institute of Technology Madras, Chennai, India

ARTICLE INFO

Keywords:
Cutoff walls
Subsurface dams
Resilience
Vulnerability
Hydrological stresses
Threshold behavior

ABSTRACT

Coastal aquifers are increasingly threatened by saltwater intrusion (SWI) driven by climate change-induced sea-level rise (SLR) and anthropogenic freshwater decline (FWD). Although physical barriers such as cutoff walls (COWs) and subsurface dams (SSDs) are widely used to mitigate SWI, their performance under hydrological stresses such as SLR and FWD remains underexplored. In this study, four widely investigated field-scale conceptual aquifers are used to systematically evaluate the resilience and vulnerability of COWs and SSDs to these hydrological stresses under contrasting inland boundary conditions. Numerical simulations with the variable-density SEAWAT model show that inland boundary conditions strongly control barrier performance. Barriers remain largely resilient under flux-controlled (FC) conditions but become vulnerable under head-controlled (HC) conditions. Under HC conditions across a range of stress levels, COWs provide consistent mitigation benefits. However, SSDs exhibit distinct threshold behavior: they remain effective up to a critical stress level, beyond which their performance rapidly deteriorates. Model simulations reveal synergistic amplification under the combined effects of SLR and FWD, wherein SWI magnitudes far exceed the sum of their individual impacts. Furthermore, vulnerability maps are developed to delineate resilient and vulnerable regimes of barrier performance across a range of hydrological stress scenarios. These findings highlight the boundary-condition-dependent, threshold-driven, and synergistic amplification of barrier vulnerability, underscoring the need to explicitly account for combined climatic and anthropogenic stresses in the design of coastal groundwater protection strategies.

1. Introduction

An estimated 1 billion people (≈12% of the global population) live within 10 km of the coastline and are categorized as ultra-coastal population (Reimann et al., 2023; Cosby et al., 2024). Approximately 30%–50% of this population depends directly or indirectly on coastal groundwater aquifers for their freshwater needs (Wada et al., 2010; Taylor et al., 2012). However, sea-level rise (SLR) due to anthropogenic climate change, and freshwater decline (FWD) due to (i) distributed pumping (Wada et al., 2010; Konikow, 2011), and/or (ii) reduced groundwater recharge due to changes in land use–land cover and precipitation patterns (Scanlon et al., 2007; Green et al., 2011) have progressively degraded both the quantity and quality of coastal groundwater aquifers over recent decades (Werner et al., 2013; Voldoire et al., 2013; Morgan, 2024). One of the primary mechanisms driving this degradation is saltwater intrusion (SWI), a process in which dense seawater migrates landward into freshwater aquifers (Chang et al., 2011; Werner et al., 2013; Voldoire et al., 2013).

Several control measures have been proposed to mitigate, or in some cases reverse, SWI in coastal aquifers (Werner et al., 2013; Abd-Elaty et al., 2024). These measures are broadly classified into (i) hydraulic control measures and (ii) physical control measures. Hydraulic control measures regulate groundwater flow by altering hydraulic heads and gradients (Abarca et al., 2006; Fang et al., 2023), and include (i) freshwater aquifer injection or areal recharge (Luyun et al., 2011; Motallebian et al., 2019; Al-Yaqoubi et al., 2021), and (ii) pumping out intruded saline water using a network of wells (Kacimov et al., 2009; Pool and Carrera, 2009). In contrast, physical control measures modify aquifer properties, primarily hydraulic conductivity, by introducing low-permeability barriers that restrict the movement of freshwater and/or seawater. These include (i) cutoff walls (COWs) (Luyun et al., 2011; Kaleris and Ziogas, 2013; Armanuos et al., 2019; Shen et al., 2020; Abd-Elaty et al., 2021; Abdoulhalik et al., 2022) and (ii) subsurface dams (SSDs) (Luyun et al., 2009; Kaleris and Ziogas, 2013; Chang et al., 2019; Abd-Elaty et al., 2021; Gao et al., 2021). A summary of different studies on COWs and SSDs is presented in Table 1.

* Corresponding author at: Department of Civil Engineering, Indian Institute of Technology Madras, Chennai, India.
E-mail address: venkatraman@iitm.ac.in (V. Srinivasan).

https://doi.org/10.1016/j.jconhyd.2026.105052
Received 27 March 2026; Received in revised form 3 July 2026; Accepted 11 July 2026
Available online 21 July 2026
0169-7722/© 2026 Elsevier B.V. All rights are reserved, including those for text and data mining, AI training, and similar technologies.

The design, performance, and evaluation of both hydraulic and physical control measures under a given hydrological condition have been extensively characterized using indicators such as (i) repulsion ratio (Luyun et al., 2011; Kaleris and Ziogas, 2013; Abdoulhalik and Ahmed, 2017; Armanuos et al., 2019), (ii) salt mass ratio (Gao et al., 2021; Chang et al., 2020; Shen et al., 2020; Zheng et al., 2021), (iii) salt area ratio (Chang et al., 2020), etc. However, the performance of these control measures can be significantly affected under altered hydrological conditions (e.g., SLR, over-extraction, and reduced recharge). Compared to physical control measures, hydraulic control measures offer greater operational flexibility, as pumping and injection rates can be adjusted in response to changing hydrological conditions. In contrast, physical control measures have limited adaptability once installed. Therefore, this study focuses on evaluating the performance of physical control measures, specifically COWs and SSDs.

COWs are typically installed in the upper aquifer regions along the coastline and act as low-conductivity barriers to groundwater flow. COWs can be made using slurry trenches (Luyun et al., 2011), concrete walls (Shen et al., 2020; Abd-Elaty et al., 2021), or sheet piles (Kaleris and Ziogas, 2013; Armanuos et al., 2019). They act as a barrier against SWI by constricting the freshwater discharge area, thereby increasing flow velocities and enhancing saltwater flushing (Luyun et al., 2011; Chang et al., 2020). Several experimental and modeling studies have investigated the effectiveness of COWs in mitigating SWI in both laboratory and field cases (Table 1). These studies show that their effectiveness improves when (i) COWs are located closer to the ocean boundary than further inland (Armanuos et al., 2019; Abdoulhalik et al., 2022; Wu et al., 2023), and (ii) the height of the COWs is increased (Luyun et al., 2011; Kaleris and Ziogas, 2013; Armanuos et al., 2019; Zheng et al., 2020; Abd-Elaty et al., 2021). COWs have been successfully installed in several places, including the Jiaodong Peninsula, China (Zheng et al., 2021), Longkou City, China (Miao et al., 2019), and Yantai City, China (Chang et al., 2021), etc.

SSDs are typically installed at the bottom of the aquifer and facilitate freshwater storage in the upstream regions of the aquifer (Miao et al., 2019; Abdoulhalik et al., 2022). They prevent dense saltwater from intruding inland by restricting saltwater recirculation inside the wedge, thereby enabling freshwater to displace the residual saltwater trapped within the inland side of SSDs (Luyun et al., 2009; Zheng et al., 2021). SSDs typically consist of an impermeable wall (concrete, masonry, etc.) or a clay core (Kaleris and Ziogas, 2013) and are ideally installed downstream of recharge areas perpendicular to dominant groundwater flow lines (Luyun et al., 2009; Abdoulhalik et al., 2017). Several experimental and modeling studies have investigated the effectiveness of SSDs in mitigating SWI in both laboratory and field settings (Table 1). These studies show that the minimum height of SSDs is equal to the height of the saltwater wedge and that their effectiveness improves when (i) SSDs are located closer to the ocean boundary than further inland (Luyun et al., 2009; Abdoulhalik et al., 2017), and (ii) the height of SSDs is increased (Chang et al., 2019; Gao et al., 2021). SSDs have been successfully installed in several locations, including San Fernando, USA (Talbot et al., 2024); Okinawa, Fukui, Kagoshima, Iwate, and Nagasaki in Japan (Nishigaki et al., 2004; Ishida et al., 2011); and Namsong, Okisong, Gocheon, and Ssangcheon in South Korea (Nishigaki et al., 2004; Ishida et al., 2011). In addition to these well-documented cases, SSD installations have also been reported in several other regions, including Burkina Faso, Ethiopia, Brazil, Tanzania, and Kenya (Nishigaki et al., 2004; Ishida et al., 2011).

The detailed literature review presented here shows that past studies on physical control measures such as SSDs and COWs have primarily focused on optimizing their location and depth under a given set of hydrological conditions (Table 1). These hydrological conditions are often based on the current/prevailing climate and anthropogenic effects. However, SLR and FWD can significantly alter hydrological conditions, which may, in turn, affect the performance of these physical barriers. The behavior of physical control measures (COWs and SSDs) under altered hydrological conditions (SLR and FWD) and contrasting inland freshwater boundary conditions remains largely unexplored.

This paper presents a systematic field-scale modeling study to assess the resilience and vulnerability of physical control measures under future climate change and anthropogenic impacts simulated through SLR and FWD. This is accomplished through four field-scale example problems: case (i) Pioneer Valley unconfined aquifer, Australia, case (ii) Willunga Basin unconfined aquifer, Australia, case (iii) Madras confined aquifer, India, and case (iv) Gaza unconfined aquifer, Palestine. The SWI and saltwater recession behavior of the physical barriers (COWs and SSDs) are characterized under SLR, FWD, and combined SLR+FWD under both head-controlled (HC) and flux-controlled (FC) inland boundary conditions. Analysis is performed under both steady and transient conditions to quantify the response times of SWI and saltwater retreat under these conditions. Additionally, vulnerability maps are generated for the different physical control measures that characterize hydrological stresses into resilient and vulnerable regimes.

2. Methodology

2.1. Details of the example problems

Four widely studied simplified field-scale example problems are employed in this study (Table 2). These include: case (i) Pioneer Valley unconfined aquifer, Australia (Chang et al., 2011; Lu and Werner, 2013), case (ii) Willunga Basin unconfined aquifer, Australia (Morgan et al., 2013), case (iii) Madras confined aquifer, India (Sherif and Singh, 1999), and case (iv) Gaza unconfined aquifer, Palestine (Moe et al., 2001). All these aquifers were simplified as horizontally oriented, homogeneous aquifers of uniform thickness with a vertical beach face. While unconfined aquifers have a low-permeability aquitard (modeled as a no-flow boundary) at the bottom boundary, confined aquifers have low-permeability aquitards (modeled as a no-flow condition) at both the top and bottom boundaries. For comparative analysis, in some of the simulations, the case (i) Pioneer Valley aquifer was modified as a confined aquifer, with due acknowledgment.

For all four example problems considered, the ocean boundary was modeled as a specified head boundary condition with a head value h_s and a specified saltwater concentration C_s. Depending on the type of inland boundary condition, the freshwater boundary was modeled either as a specified head boundary (HC) with a head value h_f or a specified flux boundary (FC) with a flux value q_f. The flux was uniformly distributed over the entire vertical extent of the freshwater boundary. The salt concentration for the freshwater boundary was set to $C_f = 0$. To facilitate inter-comparison between simulations under HC and FC conditions, the steady-state solution under the base-case (no SLR or FWD), no CM (no control measure) scenario was kept identical between the two conditions. This was achieved by first simulating the saltwater wedge under HC conditions (to steady state and in the absence of CM) and then using the resulting output to determine the flux at the freshwater boundary. This freshwater boundary flux was then used as q_f for the FC simulations. SLR simulations were performed by increasing h_s to the desired value, while FWD simulations were performed by decreasing q_f or h_f to the desired value. SLR and FWD simulations were performed by changing h_s and q_f or h_f under two conditions: (i) instantaneous change, and (ii) gradual linear change over 100 years.

COWs and SSDs are modeled as vertically oriented impermeable barriers (hydraulic conductivity $K = 0$). While the locations of COWs and SSDs from the ocean boundary (x_b) were chosen arbitrarily (within a reasonable range of values), their corresponding depths (d_b) were optimized for SSD simulations. Specifically, d_b was made equal to the height of the 50% salinity concentration contour. To facilitate inter-comparison, COWs and SSDs have the same x_b and d_b. A conceptual diagram illustrating the performance of confined and unconfined coastal aquifers with COWs and SSDs under changing climatic conditions is shown in Fig. 1.

Table 1
Summary of past field-scale and laboratory-scale studies on COW and SSD optimization and performance.

	Aquifer	Scale	Study	Optimal parameters	Reference
COW	Unconfined	Lab	Experiment + SEAWAT	x_b, d_b	Luyun et al. (2011)
	Confined	Lab	SUTRA	x_b, d_b	Kaleris and Ziogas (2013)
	Unconfined	Lab	Experiment + SEAWAT	d_b	Armanuos et al. (2019)
	Unconfined	Lab	SEAWAT	x_b, d_b	Armanuos et al. (2020)
	Unconfined	Field	SEAWAT	x_b, d_b	Armanuos et al. (2020)
	Unconfined	Lab	Experiment + SUTRA	x_b, d_b	Shen et al. (2020)
	Confined	Lab	SEAWAT	d_b	Abd-Elaty et al. (2021)
	Confined	Lab	SEAWAT	θ	Abd-Elaty et al. (2022)
	Confined	Field	SEAWAT	θ	Abd-Elaty et al. (2022)
SSD	Unconfined	Lab	Experiment + SEAWAT	d_b	Luyun et al. (2009)
	Unconfined	Lab	Experiment + SEAWAT	d_b	Abdoulhalik et al. (2017)
	Unconfined	Lab	Experiment + SEAWAT	x_b, d_b	Chang et al. (2019)
	Confined	Field	SEAWAT	d_b	Chang et al. (2020)
	Confined	Lab	SEAWAT	d_b	Abd-Elaty et al. (2021)
	Confined	Lab	SEAWAT	θ	Abd-Elaty et al. (2022)
	Confined	Lab	SEAWAT	d_b	Abd-Elaty et al. (2021)
	Confined	Lab	SEAWAT	θ	Abd-Elaty et al. (2022)
	Confined	Field	SEAWAT	θ	Abd-Elaty et al. (2022)

Table 2
Model parameters (base-case scenario) for the field-scale confined/unconfined aquifer problems used in this study. Model parameters were adapted from Chang et al. (2011) and Morgan et al. (2015).

Description	Symbols and units	Case 1 Pioneer	Case 2 Willunga	Case 3 Madras	Case 4 Gaza
Aquifer length	x_0 (m)	1000	3500	2600	10 000
Aquifer thickness	z_0 (m)	30	24	30	120
Effective porosity	η_e (–)	0.35	0.2	0.35	0.2
Specific storage	S_s (m^{-1})	1×10^{-5}	1×10^{-5}	1×10^{-5}	1×10^{-5}
Specific yield	S_y (–)	0.1	0.2	0.1	0.2
Hydraulic conductivity	K (m day^{-1})	10	10	260	15
Saltwater boundary head	h_s (m)	30	20	30	100
Freshwater boundary head	h_f (m)	31.5	23	31	112
Freshwater boundary flux	q_f (m^2 day^{-1})	0.3409[a]	0.1696	1.0	1.7996
x-dispersivity	α_x (m)	1	1	66.6	10
y-dispersivity	α_y (m)	0.1	0.1	6.6	1
z-dispersivity	α_z (m)	0.01	0.01	0.66	0.1
Saltwater concentration	C_s (kg m^{-3})	35	35	35	35
Freshwater concentration	C_f (kg m^{-3})	0	0	0	0
Saltwater density	ρ_s (kg m^{-3})	1025	1025	1025	1025
Freshwater density	ρ_f (kg m^{-3})	1000	1000	1000	1000
Recharge rate	W (m day^{-1})	0	0	0	0
COW or SSD location	x_b (m)	100	100	200	300
COW or SSD depth	d_b (m)	13	8	13	45
x-mesh length	Δx (m)	10	10	5	10
y-mesh length	Δz (m)	1	1	1	1

[a] For the case of Pioneer-Valley unconfined aquifer $q_f = 0.3523$ m^2 day^{-1} was used under FC conditions.

2.2. Numerical modeling procedure

Simulations were performed using the coupled variable-density groundwater flow and transport model SEAWAT, which simulates the transient mixing behavior at the saltwater–freshwater interface (Langevin et al., 2008). The flow equations were solved using the preconditioned conjugate gradient solver with the well and recharge packages. The advection term was solved using the third-order ultimate Total Variation Diminishing (TVD) scheme, coupled with an implicit dispersion scheme and a source/sink package, employing an operator-splitting approach to solve the full transport equations. The coupled density-dependent flow problem was solved using the variable density flow (VDF) package. A uniform grid spacing of $\Delta z = 1$ m was used in the z-direction for all problems. In confined aquifer cases, all the layers are represented as confined cells. In unconfined aquifer cases, all layers except the top layer are represented as confined cells. The top layer in unconfined aquifers was modeled using 3 m thick convertible cells. A uniform grid size of Δx was employed along the x-direction, with the value of Δx being case-dependent to achieve grid convergence (Table 2). Δy was fixed as 1 m to simulate a two dimensional problem (along the x- and z-directions) with a unit width along the y-direction.

For the case of instantaneous SLR and FWD, transient simulations were run until steady state using a single stress period with 118 time steps and a time-step multiplier of 1.1. To simulate gradual SLR and FWD, transient simulations were run until steady-state using 101 stress periods with 100 time steps, and a time-step multiplier of 1. While the first 100 stress periods were used to apply the gradually varying SLR/FWD, the last (101st) stress period was used to simulate the aquifer response post-stress (SLR/FWD) application. For the gradual SLR case, a 0.05 m y^{-1} SLR rate was considered, while for the gradual FWD case, a 0.5% y^{-1} reduction in q_f was considered.

The Dirichlet ocean head boundary condition (h_s) was modeled using the CHD package, with a specified saltwater concentration (C_s) modeled using the CHD option in the SSM package. Under HC conditions, the freshwater boundary was modeled as a Dirichlet boundary (h_f) using the CHD package, with a specified freshwater concentration ($C_f = 0$) using the CHD option in the SSM package. Under FC conditions, the freshwater boundary was modeled using the WEL package, with boundary nodes represented as injection wells with q_f equally distributed among them. q_f represents the flux per unit width (along the y-direction) of the aquifer and has units of m^2 day^{-1}. A clean, salt-free aquifer was used as the initial condition for the base-case with no

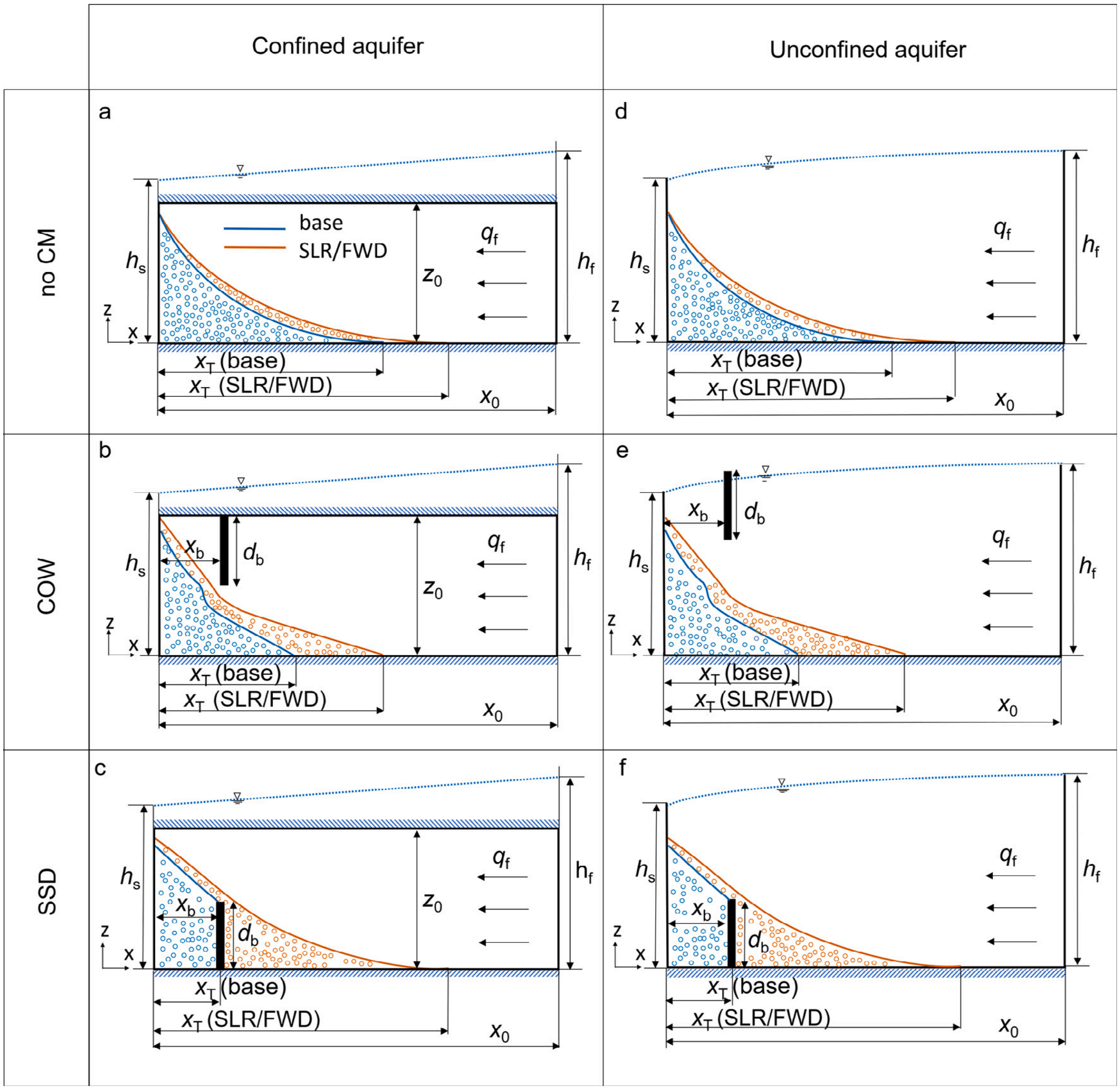

Fig. 1. Conceptual model of a coastal aquifer performance with physical control measures such as COWs and SSDs under the influence of SLR/FWD.

CM scenario. The steady-state solutions obtained from the base-case scenarios were used as the initial conditions for simulating the COW and SSD cases. Similarly, the steady-state solutions from the no CM, COW, and SSD simulations under the base cases were used as initial conditions for the SLR and FWD simulations.

To evaluate the robustness of the model, a sensitivity analysis was conducted using the case (i) Pioneer Valley confined aquifer example. The analysis examined the influence of variations in aquifer and barrier properties under different SLR (HC conditions) and FWD scenarios by varying the values of h_s and h_f and q_f respectively. Aquifer parameters, including K, α_x, and S_s, were varied by one order of magnitude above and below their baseline values. η_e was varied by ± 0.1 relative to its baseline value, while z_0 was reduced by 5 m and 10 m from the reference case. Barrier parameters, x_b and d_b, were varied by ± 5 m and ± 50 m, respectively, from their respective baseline values.

2.3. Quantifying interaction effects

Under the combined effects of SLR and FWD, the interaction effect between SLR and FWD on x_T is quantified using a relative synergy index (RSI). RSI is defined as:

$$\mathrm{RSI} = \frac{\Delta x_{\mathrm{T,\ combined}} - \left(\Delta x_{\mathrm{T,\ SLR}} + \Delta x_{\mathrm{T,\ FWD}}\right)}{\Delta x_{\mathrm{T,\ combined}}} \quad (1)$$

where Δx_T represents the increase in toe length compared to the base case (no SLR or no FWD) scenario.

RSI $>$ 0 represents a synergistic (positive) interaction behavior, while RSI $<$ 0 represents an antagonistic (negative) interaction behavior. RSI = 0 represents purely additive behavior (no interaction effects), while RSI = 1 represents a purely interaction-driven synergistic behavior.

3. Results and discussion

3.1. Performance of control measures under the base case

Model simulations performed on the Pioneer Valley aquifer for the base-case scenario (no SLR and no FWD) and in the absence of control measures (no CM) show that the steady-state salt wedge toe length (x_T) intrudes inland up to 280 m from the coastline (Fig. 2a, *solid blue line*). When a COW is added, the salt wedge retreats significantly towards the sea, reducing x_T to 219 m and 230 m under FC and HC conditions, respectively (Fig. 2a and d, *dotted blue lines*). When an SSD is added, the salt wedge also retreats significantly towards the sea, reducing x_T from 280 to 100 m (Fig. 2b and c, *dashed blue line*). The location of the salt wedge toe coincides with the location of the SSD, i.e., $x_T = x_b$. The seaward retreat of x_T in the presence of SSDs and COWs is attributed to changes in the aquifer hydraulic conductivity and flow fields. While

COWs constrict the freshwater discharge area, thereby increasing flow velocities and enhancing saltwater flushing (Luyun et al., 2011; Chang et al., 2020; Zheng et al., 2022), SSDs restrict the saltwater recirculation inside the wedge, thereby enabling freshwater to displace the residual saltwater trapped within the inland side of SSDs (Luyun et al., 2009; Zheng et al., 2021). A similar behavior was also observed in unconfined aquifers (Fig. S1).

3.2. Performance of control measures under SLR

When subjected to a 0.5 m SLR, the behavior of COWs and SSDs differs depending on the inland freshwater boundary condition (FC or HC). Simulations using FC inland boundary conditions show that the steady-state x_T remains unchanged between the base-case and the SLR case under both COW and SSD control measures (Fig. 2a and b, *dotted and dashed red lines*). This is expected because, in the absence of control measures (no CM), FC aquifers do not show appreciable additional SWI due to SLR (Chang et al., 2011; Sun et al., 2017). This lack of additional SWI is attributed to the head-lift effect (Chang et al., 2011; Sadhasivam et al., 2025) whereby freshwater heads (h_f) rise in proportion to SLR and maintain the hydraulic head difference ($\Delta h = h_f - h_s(1+\delta)$; where $\delta = (\rho_s - \rho_f)/\rho_f$) between the fresh and saltwater boundaries (Chang et al., 2011; Sun et al., 2017; Sadhasivam et al., 2025). Additional simulations performed over a range of SLR values (0 to 0.5 m) for the no CM, COW, and SSD cases indicate that h_f increases linearly with SLR (Fig. 2c, *green lines*) while the toe positions remain unchanged (Fig. 2c, *black lines*). These results suggest that control measures maintain their effectiveness and are highly resilient to SLR under FC inland freshwater boundary conditions. Unconfined aquifers show a similar behavior to that observed in confined aquifers (Fig. S1).

For a given SLR value, h_f for COWs and SSDs shows contrasting behavior relative to the no CM case (Fig. 2c, *green lines*). Under FC conditions, relative to the no CM case, COW increases h_f, SSD decreases h_f. These findings are consistent with the previously published results by Chang et al. (2023). This is because COWs decrease the hydraulic conductivity in the upper freshwater aquifer zone. Therefore, to maintain a constant q_f, the hydraulic gradient has to increase to compensate for the decline in conductivity. This increase in hydraulic gradient is achieved by increasing h_f. SSDs, on the other hand, reduce hydraulic conductivity in the lower saltwater aquifer zone, hindering the saltwater wedge from intruding into the freshwater aquifer. Therefore, a lower hydraulic gradient is sufficient to maintain the same q_f. These simulations suggest that while both COWs and SSDs are resilient to SLR under FC conditions, SSDs can achieve this with a smaller h_f compared to COWs.

Under HC inland freshwater boundary conditions, SLR induces significant additional SWI of 221, 193, and 381 m for the no CM, COW, and SSD cases, respectively (Fig. 2d and e, *red lines*). This additional SWI under HC conditions is attributed to the flux-decline effect (Carretero et al., 2013; Sadhasivam et al., 2025). Under these conditions, the hydraulic head difference Δh and gradient between the fresh and saltwater boundaries decrease in response to SLR. The decrease in hydraulic gradient reduces freshwater boundary flux (q_f), thereby inducing a flux-decline effect (Fig. 2f, *green lines*). For a 0.5 m SLR, while COWs largely retain their effectiveness as a control measure, SSDs completely fail (Fig. 2e and f). Simulations performed with COWs over a range of SLR values (0 to 0.5 m) show that, although x_T increases with SLR, the benefit of using COWs is largely retained, i.e., the difference in x_T between no CM and COW does not decrease as SLR increases (Fig. 2f, *solid* and *dotted black lines*). This behavior is also reflected in the q_f variation with SLR (Fig. 2f, *solid* and *dotted green lines*).

Simulations performed with SSDs over a range of SLR values (0 to 0.5 m) show a threshold behavior, wherein x_T remains constant (i.e., $x_T = x_b$) up to a SLR value of 0.38 m (Fig. 2f, *dashed black line*). Within this range, SSDs exhibit excellent resilience to SLR. However, when SLR > 0.38 m, SSDs are not a reasonable control measure and their x_T is close to the no CM case. This threshold behavior is also observed in q_f (Fig. 2f, *dashed green line*), where the q_f of SSD matches the q_f of no CM beyond the threshold SLR value of 0.38 m. Note that the threshold was identified as the value of SLR at which $x_T > x_b$. These simulations show that under HC conditions, while SLR reduces the performance of COWs, it is still effective as a control measure. SSDs, on the other hand, show a biphasic response, remaining highly resilient below the threshold SLR value but becoming highly vulnerable (ineffective) beyond it. A similar behavior was also observed in unconfined aquifers (Fig. S1 d, e, and f).

COWs and SSDs show contrasting q_f responses to SLR under HC conditions (Fig. 2f, *green line*). For a given SLR, compared to the no CM case, q_f decreases under COW and increases under SSD. Similar behavior has been reported by others (Fang et al., 2023). This is attributed to the aquifer location, where the control measure decreases the hydraulic conductivity. For COWs, hydraulic conductivity decreases in the upper freshwater zone. Since this is the primary location of freshwater flux discharge into the ocean, q_f decreases as hydraulic conductivity is reduced while maintaining the same hydraulic gradient (Δh). This is advantageous, as the salt wedge retreat is accompanied by a decline in q_f, resulting in reduced freshwater discharge into the ocean. SSDs, on the other hand, decrease hydraulic conductivity in the lower saltwater zone. In this situation, q_f increases as h_f remains constant. This implies that, while SSDs are effective in reversing SWI, they also cause an undesirable increase in freshwater discharge into the ocean under HC conditions.

Transient simulations show significant differences in time scales of the saltwater wedge movement between COWs and SSDs (Fig. 3). Under the base case scenario (no SLR), while COW results in x_T receding to its steady-state value in a couple of decades, SSD takes more than two centuries for x_T to reach its steady-state value under both HC and FC conditions (Fig. 3 *blue lines*). The prolonged transient behavior observed under SSDs is attributed to the following reasons. (i) The hydraulic gradients and the associated groundwater velocities in the residual saltwater wedge zone that remains on the upstream (freshwater) side of SSD are very low. Therefore, its flushing takes a much longer time (Luyun et al., 2009; Zheng et al., 2021). (ii) Flushing involves lifting the saltwater upwards and over the SSD. This can be accomplished only when the flush water concentration is low (less than 10% of seawater concentration). Concentrations above this level must first be diluted by mixing, then lifted over the barrier (Zheng et al., 2021). (iii) The magnitude of x_T retreat is greater for SSDs compared to COWs, requiring a larger volume of the aquifer to be flushed (Fig. 3).

When subjected to a 0.5 m instantaneous SLR under FC conditions, SSDs show prolonged transients in SWI compared to COWs (Fig. 3c and d). While COWs take about 100 years to reach steady state conditions, SSDs take more than 400 years. Compared to the no CM case, COWs do not alter the time-scales of the transient saltwedge movement (Fig. 3c). However, SSDs significantly prolong the transient response compared to the no CM case. This can be advantageous as SSDs slow the rate of SWI due to SLR. Furthermore, within the threshold SLR of 0.38 m, there is no additional SWI in SSDs, whereas COWs experience additional SWI. In contrast to x_T, h_f and q_f show rapid (a few days) transient responses under both COW and SSD (Fig. S3). The transient behavior of unconfined aquifers is similar to that observed in confined aquifers, with the SSD threshold also occurring at an SLR of 0.38 m (Fig. S2). Transient simulations for gradually increasing SLR also show similar behavior, with SSDs exhibiting prolonged transients compared to COW (Fig. S4).

These simulations show that under FC conditions, both COWs and SSDs are resilient to SLR. However, under HC conditions, while COWs show continued resilience, SSDs exhibit a biphasic behavior, wherein they are highly resilient when SLR < threshold value and highly vulnerable when SLR > the threshold. Additionally, SSDs exhibit prolonged (century-scale) transients under both intrusion and retreat scenarios, with respect to x_T, while the time-scales of intrusion and retreat for COWs are shorter (decadal-scale).

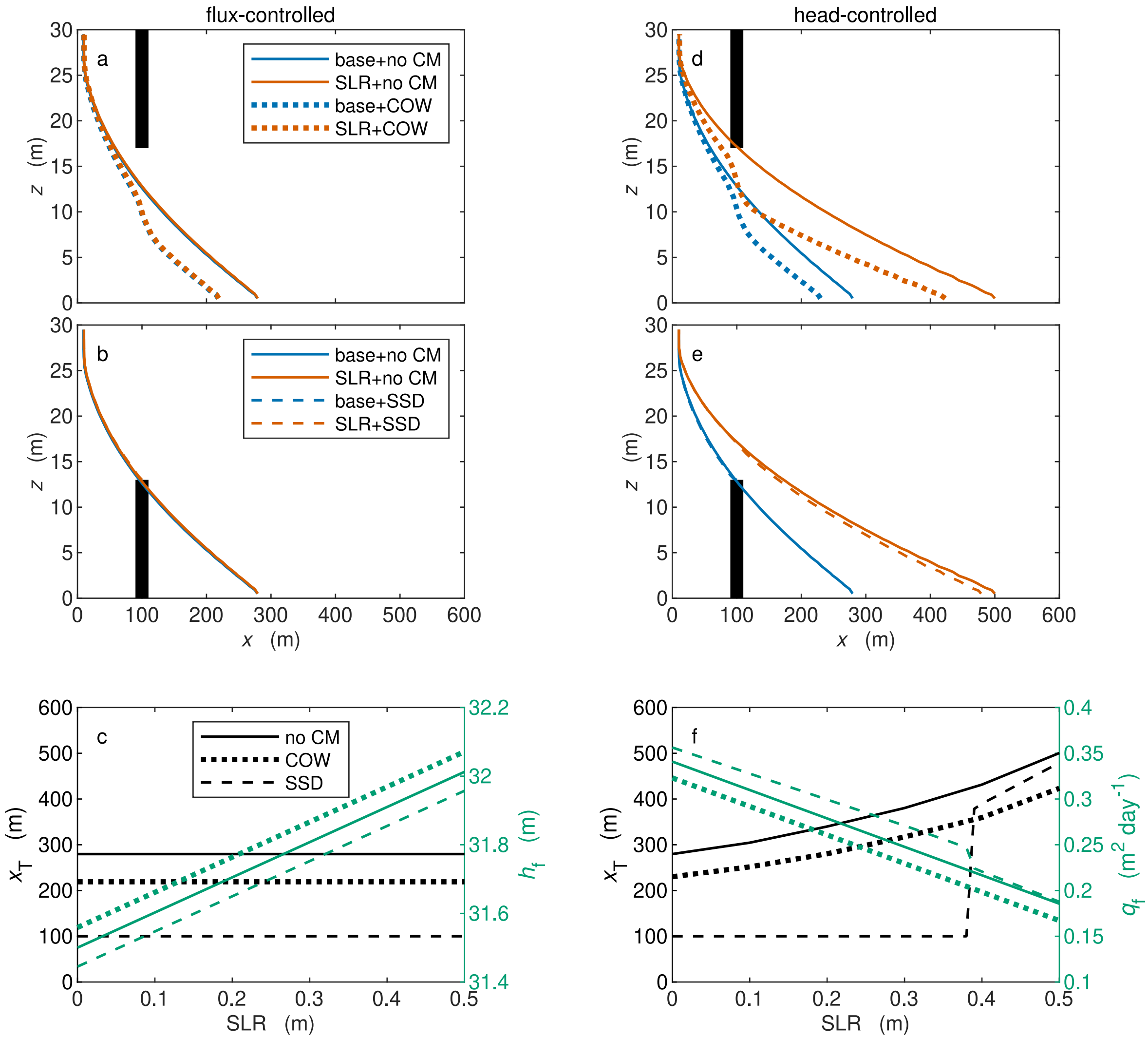

Fig. 2. Steady-state model simulations showing the effect of SLR-induced SWI in case (i) Pioneer Valley confined aquifer in the presence of COW or SSD. 50% saltwater concentration (0.5 C_s) contour lines under base case and 0.5 m SLR for COW and SSD under FC conditions (a) and (b), and under HC conditions (e) and (f). Effect of variation of SLR on (c) freshwater head (h_f), and toe-location (x_T) under FC conditions, and (f) freshwater flux (q_f), and toe location (x_T) under HC conditions, respectively.

3.3. Performance of control measures under FWD

When subjected to a 50% decline in freshwater flux (realized through reductions in q_f), additional SWIs of 266, 197, and 437 m are observed for no CM, COW, and SSD cases, respectively (Fig. 4a and b). At this level of FWD, COWs largely retain their effectiveness as a control measure, while SSDs completely fail. This is because the FWD magnitude is higher than the threshold for SSDs. i.e., a 50% reduction in q_f corresponds to a decline in freshwater head h_f of 0.56 m, and this value is more than the 0.38 m threshold for SSD (Fig. 2f *dashed lines*). Simulations performed over a range of FWD show that the SSD threshold occurs at 27.6% reduction in q_f (Fig. 4c, *dashed green line*), which corresponds to the 0.38 m h_f threshold. When FWD is within this threshold, SSDs show no additional SWI. Model simulations of FWD realized through reductions in h_f exhibit a similar behavior to that of SLR simulations under HC conditions. This is because changes in either h_s (due to SLR) or h_f (due to FWD) alter Δh, which in turn causes a change in gradient and hence SWI.

Transient simulations under FWD (Fig. S5) show behavior similar to that observed under SLR, with SSDs exhibiting prolonged transients (century-scale) compared to COWs (decadal-scale). A similar behavior was also observed in unconfined aquifers (Figs: S13 and S14). Transient simulations performed for gradually increasing FWD also show similar behavior, with SSDs exhibiting prolonged transients compared to COWs (Fig. S15). These simulations show that under FWD, COWs exhibit continued resilience. However, SSDs exhibit a biphasic behavior, wherein they are highly resilient when FWD < the threshold value and highly vulnerable when FWD > the threshold.

3.4. Sensitivity analysis

Sensitivity analysis simulations show that the resilience and vulnerability of COWs and SSDs are relatively insensitive to aquifer parameters K, η_e, and S_s (Figs. S6, S7, and S8). In all these simulations, the steady-state x_T values remain unchanged over the range of SLR and FWD values under both COW and SSD cases. These findings are consistent with previously published results in the absence of control measures (Sadhasivam et al., 2025). On the other hand, barrier performance is significantly affected by aquifer parameters α_x, and z_0 (Figs. S9 and S10). Increasing α_x enhances mixing of fresh and saltwater and reduces x_T under both COW and SSD cases, indicating that physical barriers are more resilient under aquifers with high dispersivity. In fact, model simulations indicate that when α_x is increased by an order of magnitude, the threshold failure behavior of SSDs completely vanishes

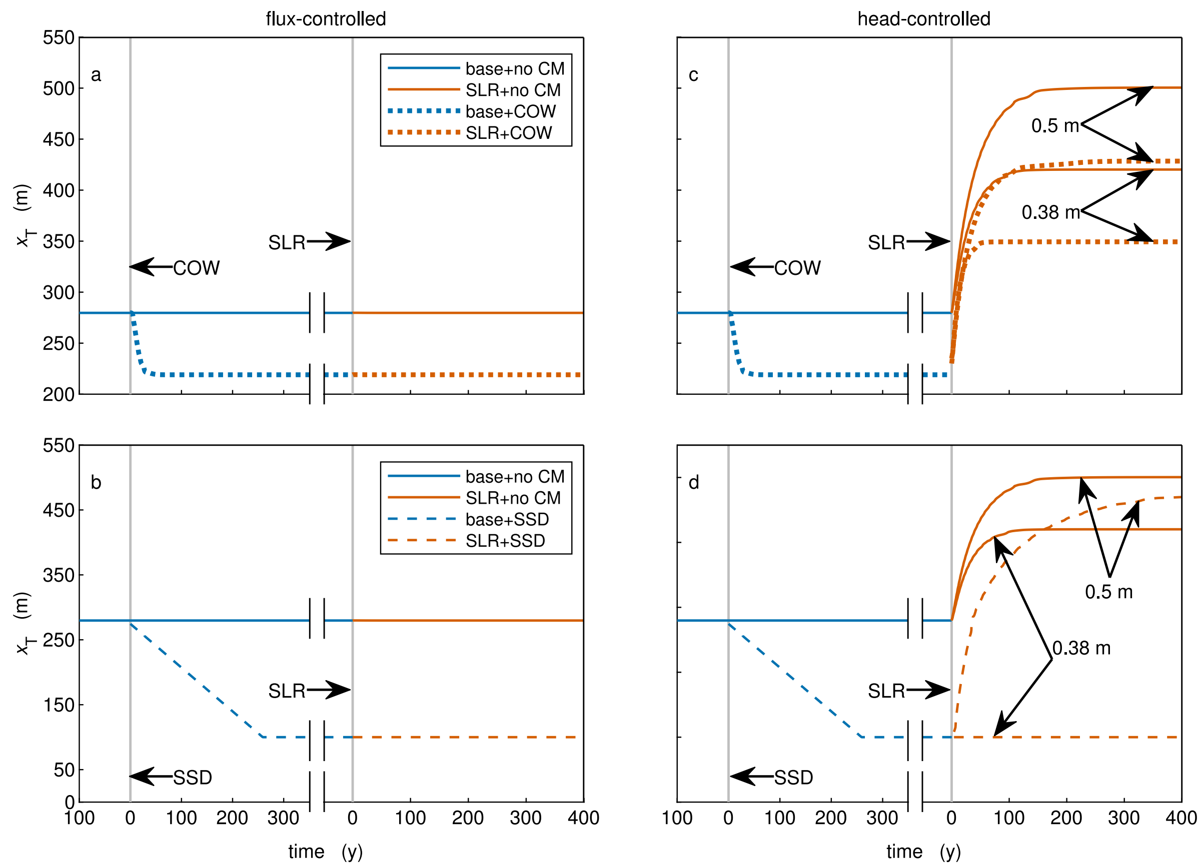

Fig. 3. Transient model simulations showing the effect of instantaneous SLR (0.5 and 0.38 m) induced SWI in case (i) Pioneer Valley confined aquifer in the presence of COW (a) and (c) or SSD (b) and (d). Grey vertical lines show the onset of control measure (COW or SSD) or SLR.

for the range of SLR and FWD considered (Fig. S9 e and f). Similarly, as the aquifer thickness decreases, barrier resilience to SLR and FWD increases (Fig. S10). This is because, as z_0 decreases (while d_b is maintained constant) the ratio of barrier height to aquifer thickness (d_b/z_0) increases, resulting in better barrier resilience.

Barrier properties x_b and d_b significantly influence barrier performance under both SLR and FWD (Figs. S11 and S12). Decreasing d_b reduces barrier performance, making the aquifer more vulnerable to SLR and FWD, whereas increasing d_b enhances barrier resilience. This trend is observed for both COWs and SSDs and is attributed to the influence of (d_b/z_0) on barrier performance, as discussed earlier. In contrast, variations in x_b show contrasting trends depending on whether the performance is assessed with respect to COWs or SSDs (Fig. S12). Moving the barrier closer to the shoreline (lower x_b) increases the resilience of COWs but decreases that of SSDs, whereas, moving the barrier farther away from the shoreline (higher x_b) has the opposite effect. Therefore, although both COWs and SSDs benefit from larger d_b, COWs are more resilient under lower x_b values, while SSDs are more resilient under higher x_b values. These findings are consistent with previously published results (Chang et al., 2019; Armanuos et al., 2020).

3.5. Performance of control measures under the combined effects of SLR and FWD

Under the combined effects of SLR and FWD, aquifers experience significant additional SWI (Δx_T, which represents additional SWI compared to the case of no SLR or FWD). This additional SWI exceeds the sum of the individual effects of SLR and FWD, with or without the presence of control measures (Fig. 5). This is attributed to the non-linear SWI response of the aquifer to increasing hydrological stresses (SLR or FWD) (Sherif and Singh, 1999; Sadhasivam et al., 2025). For example, SLR simulations for the no CM case show that, compared to the base case scenario, a 0.1 m SLR results in an additional SWI of 25 m while a 0.2 m SLR results in an additional SWI of 60 m, which exceeds twice the increase caused by a 0.1 m SLR (2 × 25 = 50 m) (Fig. 2f, *solid black line*). A similar non-linear synergistic amplification behavior is observed when combining different types of stress, such as SLR and FWD.

Model simulations under no CM conditions show that the degree of synergistic amplification increases with the severity of SLR and FWD (Fig. 5a). Model simulations show that COWs remain effective in partially mitigating additional SWI due to SLR, FWD, and the combined effects of SLR and FWD (Fig. 5b). The Δx_T values of COWs are significantly smaller than those of the no CM case. However, under the combined effect of SLR and FWD, COWs show significant additional SWI as compared with only SLR or FWD alone. The sum of Δx_T values for SLR and FWD cases is much smaller than the Δx_T of the combined case due to the synergistic amplification effects discussed earlier (Fig. 5b). Unlike COWs, SSD simulations show that under the combined effects of SLR and FWD, the threshold behavior of SSDs is exemplified (Fig. 5c). For example, under 0.2 m SLR with a 20% reduction in FWD, while the individual effects do not cause any additional SWI, the combined effect results in an additional SWI of 284 m. Similar behavior with significant additional SWI under combined effects is observed for other SLR and FWD combinations. Notably, the additional SWI in the SSD case is often greater than that in the no CM case (Fig. 5c). This is because, while SSDs perform better than the no CM case within the threshold, they perform as poorly as the no CM case when the threshold is increased, resulting in larger Δx_T values. These simulations show that when the threshold value (for a given combination of SLR and FWD) is breached, SSDs behave similarly to the no CM case and fail to be effective control measures.

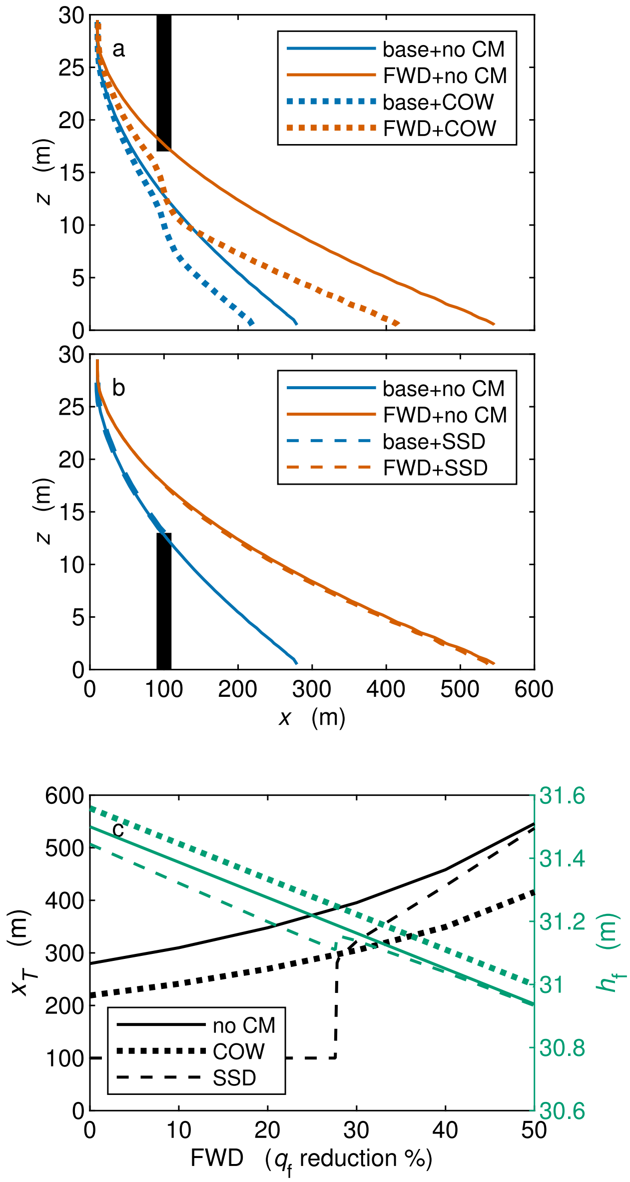

Fig. 4. Steady-state model simulations showing the effect of FWD (realized through reductions in q_f) induced SWI in case (i) Pioneer Valley confined aquifer in the presence of COW or SSD. 50% saltwater concentration (0.5 C_s) contour lines under base case and 50% FWD for COW (a) and SSD (b). Effect of variation of FWD magnitudes on (c) freshwater head (h_f), and toe-location (x_T).

RSI indicates moderate levels of synergy (0–0.5) across a range of SLR and FWD values for both the no CM and COW cases, with higher RSI values occurring under larger SLR and/or FWD magnitudes (Fig. 5d and e). The presence of COWs marginally increases the synergistic effects of combined stresses. In contrast, under SSDs, RSI values approach 1 over a significant portion of the domain, indicating predominantly synergistic interactions (Fig. 5f). Within this region (RSI = 1), neither SLR nor FWD produces additional SWI ($\Delta x_T = 0$) when applied individually, whereas their combined application results in $\Delta x_T > 0$, indicating a purely interaction-driven threshold behavior (Fig. 5f). Within the combined SLR+FWD threshold region, $\Delta x_{T,\ combined} = 0$; consequently RSI is undefined (Fig. 5f; *white* regions). These simulations show that under the combined effects of SLR and FWD, while COWs marginally increase RSI, SSDs significantly increase RSI, indicating much stronger synergistic interactions.

3.6. Vulnerability maps for control measures

Model simulations of COWs and SSDs under the combined effects of SLR and FWD for the four different field-scale problems (Table 2) reveal the resilience and vulnerability of these control measures under various situations (Fig. 6). COWs consistently reduce x_T under all combinations of SLR and FWD for all four example cases. Although SLR and/or FWD induce additional SWI, the effectiveness of COWs in pushing the saltwater wedge seaward is retained, and COWs continue to perform better than the no CM case (Fig. 6a, c, e, g).

SSDs, on the other hand, exhibit threshold behavior wherein they are effective below the threshold stress value (SLR and/or FWD) and become ineffective beyond it. The threshold envelope delineated by the dashed contour lines (Fig. 6b, d, f, and h) is an important indicator that divides the SSD response domain into resilient and vulnerable regimes. As the magnitudes of SLR and/or FWD increase beyond the threshold envelope, the effectiveness of SSDs rapidly diminishes, and they eventually perform similarly to the no CM case. These simulations demonstrate the practical applications of vulnerability maps (Fig. 6) for identifying the resilient and vulnerable operating regimes of physical control measures under future SLR and FWD scenarios.

3.7. Limitations and implications

This study was performed using homogeneous coastal aquifers with simplified geometries (vertical beach face and a horizontal bottom boundary) to investigate the effects of inland boundary conditions and hydrological stresses (SLR and/or FWD) on the performance of physical barriers. While these simplified representations help identify the dominant mechanisms controlling barrier resilience and vulnerability, real coastal aquifers are often heterogeneous, anisotropic, and subject to spatially variable recharge and complex shoreline geometries (Werner et al., 2013). In addition, the simulations were performed using two-dimensional cross-sectional models with idealized impermeable barriers, and therefore do not account for three-dimensional flow effects (Nam et al., 2025), barrier leakage, construction imperfections, or alongshore variations that may influence barrier performance in field settings.

The simulations performed in this study only considered prescribed SLR and FWD scenarios (instantaneous or linearly varying). However, future climatic and anthropogenic stresses remain uncertain, site-dependent, and time-varying. Additionally, processes such as tidal fluctuations, seasonal recharge variability, and transient localized pumping stresses (including up-coning) were not explicitly included in the present analysis (Werner et al., 2013). These factors may influence both the transient response and the threshold behavior of the control measures, particularly for SSD systems, where threshold values were found to depend strongly on hydrological conditions and aquifer properties.

Despite these simplifications, the results provide important process-level insights into the contrasting behavior of COWs and SSDs under changing hydrological stresses. In particular, the identified roles of inland boundary conditions, synergistic amplification under combined stresses, and threshold-dependent failure mechanisms are expected to remain qualitatively relevant across a broad range of coastal aquifer systems. The vulnerability maps developed in this study therefore provide a useful conceptual framework for delineating the resilient and vulnerable regimes of physical barriers and may help guide future site-specific investigations, monitoring strategies, and adaptive groundwater management under climate change.

4. Summary and conclusions

This study systematically evaluated the performance of physical barriers, namely, COWs and SSDs, in mitigating SWI in coastal aquifers under climatic and anthropogenic stresses (SLR and FWD). Numerical

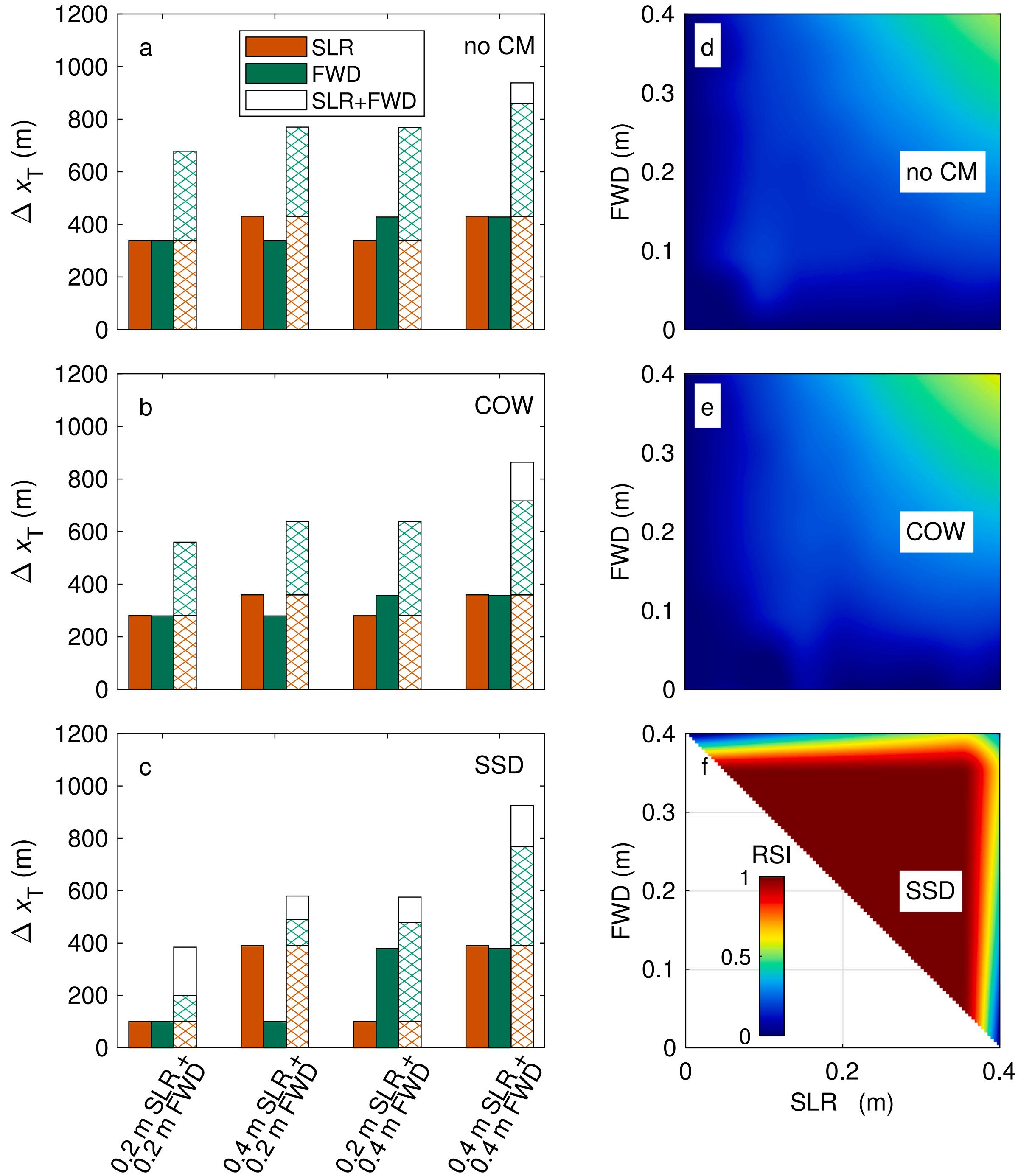

Fig. 5. Steady-state model simulations showing the individual and combined effects of SLR and FWD (realized through reductions in h_f) on additional SWI Δx_T for case (i) Pioneer Valley confined aquifer, under (a) no-control measure, (b) COW, and (c) SSD cases. *Red* and *green* bars represent the individual effects of SLR and FWD, respectively, while *white bars* represent the combined effects of SLR and FWD. The hatched *red* and *green* portions within the *white* bars show the individual contributions of SLR and FWD towards increasing x_T. The clean *white* portion of the bar represents the non-linear synergistic amplification effects. (d), (e), and (f) show the relative synergy index (RSI) under no CM, COW, and SSD cases, respectively.

simulations were performed using the coupled variable-density SEAWAT for four field-scale example problems. Using these simulations, the vulnerability and resilience of the control measures to SLR and FWD were assessed. The results demonstrate that barrier performance is strongly influenced by inland freshwater boundary conditions. Under flux-controlled (FC) systems, both COWs and SSDs exhibit resilience to SLR due to the compensatory head-lift effect. In contrast, under head-controlled (HC) systems, both SLR and FWD reduce the effectiveness of physical barriers. While COWs maintain consistent performance across a range of SLR and FWD, SSDs exhibit a distinct threshold behavior wherein they perform well when the hydrological stresses fall within a threshold value and fail abruptly (behaving similar to a no-control system) beyond it.

Transient analyses further reveal contrasting system dynamics between COWs and SSDs. While COWs respond relatively rapidly (decadal-scale) to imposed stresses, enabling quicker stabilization of saltwater intrusion fronts, SSDs exhibit prolonged transient behavior (century-scale), delaying both intrusion and retreat processes. While this delayed response can enhance short-term freshwater retention and slow intrusion rates, it may also limit adaptability under rapidly changing

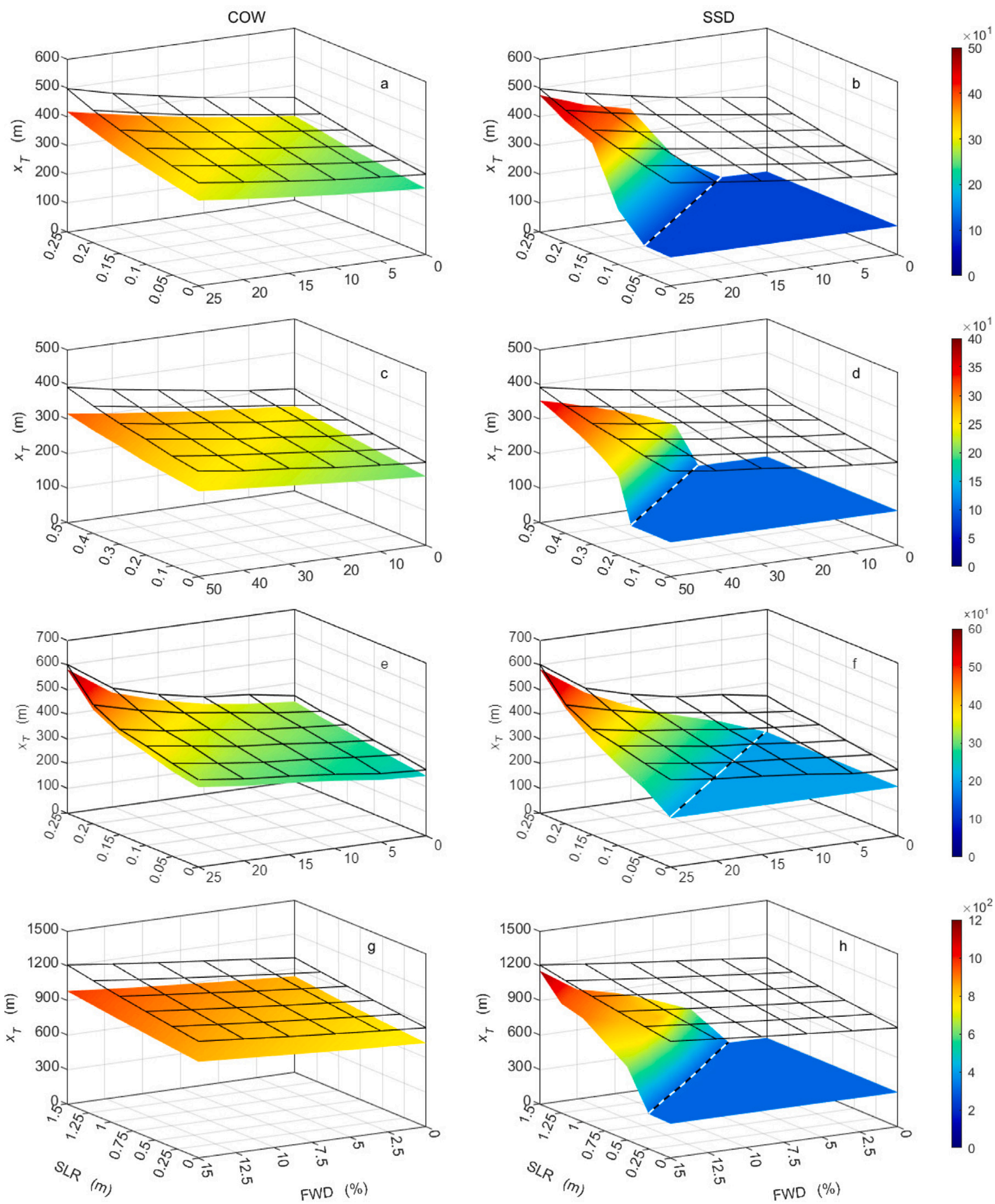

Fig. 6. Model simulated x_T values 3D surfaces due to the combined effects of SLR and FWD (realized through reductions in h_f) for COW and SSD in case (i) Pioneer valley confined aquifer, Australia (a and b), case (ii) Willunga Basin unconfined aquifer, Australia (c, and d), case (iii) Madras confined aquifer, India (e and f) and case (iv) Gaza unconfined aquifer, Palestine (g and h). Black mesh-grid surfaces represent x_T under the no CM case while the colored surfaces show x_T in the presence of COW (left column) or SSD (right column). The black and white dashed contour lines in b, d, f, and h represent the threshold envelope for SSD.

boundary conditions. These results highlight that steady-state performance alone is insufficient for evaluating control measures and that transient response time-scales constitute a critical dimension of resilience.

A key finding of this study is the synergistic amplification of the SWI response of coastal aquifers under combined SLR and FWD stresses. The combined effects of SLR and FWD produce saltwater intrusion that far exceeds the sum of their individual impacts, reflecting the non-linear behavior inherent in density-dependent flow systems. This synergistic amplification becomes more pronounced with increasing stress magnitude and can push systems across critical thresholds, particularly for SSDs, where combined stresses can trigger abrupt failure even when individual stresses remain within safe limits. These results emphasize that evaluating these stresses in isolation can significantly underestimate future risks and potentially lead to overconfidence in the long-term performance of control measures.

To address this complexity, vulnerability maps were developed that delineate regions of resilient and vulnerable system behavior across different combinations of SLR and FWD. These maps reveal that while COWs maintain consistent effectiveness across a wide range of stress conditions, SSD performance is bounded by threshold envelopes that separate resilient and vulnerable regimes. The locations of these threshold envelopes - and hence the delineation of resilient and vulnerable regimes in the vulnerability maps - depend on aquifer properties and barrier design parameters. These simulations show that vulnerability maps provide a practical, visual framework for identifying safe operating conditions, guiding design decisions, and anticipating failures under future climate scenarios.

Overall, the findings of this study underscore the importance of nonlinear synergistic amplification and threshold-dependent behavior of physical barrier performance in coastal aquifers. The interplay between boundary conditions, stress levels, and barrier type yields diverse system responses ranging from resilience to vulnerable and even complete failure. These insights highlight the need to explicitly incorporate future climate stresses, combined effects, transient aquifer response, and site-specific characteristics into the design and management of saltwater intrusion mitigation strategies using physical barriers such as COWs and SSDs.

CRediT authorship contribution statement

Rajagopal Sadhasivam: Writing – review & editing, Writing – original draft, Methodology, Conceptualization. **Venkatraman Srinivasan:** Writing – review & editing, Supervision, Methodology, Funding acquisition, Conceptualization.

Declaration of competing interest

The authors declare that they have no known competing financial interests or personal relationships that could have appeared to influence the work reported in this paper.

Acknowledgments

The authors thank the editor and the two anonymous reviewers for their thoughtful and constructive comments, which substantially improved the quality of this manuscript. This research was in part supported by the Ministry of Education, India, and the Department of Science and Technology, India via Grant No: CIE1819267DSTXKPSU.

Appendix A. Supplementary data

Supplementary material related to this article can be found online at https://doi.org/10.1016/j.jconhyd.2026.105052.

Data availability

No data was used for the research described in the article.

References

Abarca, E., Vázquez-Suñé, E., Carrera, J., Capino, B., Gámez, D., Batlle, F., 2006. Optimal design of measures to correct seawater intrusion. Water Resour. Res. 42 (9), http://dx.doi.org/10.1029/2005wr004524.

Abd-Elaty, I., Kuriqi, A., Ahmed, A., 2024. Effectiveness of different mixed physical barriers in controlling seawater intrusion in homogeneous and layered coastal aquifers. Groundw. Sustain. Dev. 27, 101318. http://dx.doi.org/10.1016/j.gsd.2024.101318.

Abd-Elaty, I., Pugliese, L., Straface, S., 2022. Inclined physical subsurface barriers for saltwater intrusion management in coastal aquifers. Water Resour. Manag. 36 (9), 2973–2987. http://dx.doi.org/10.1007/s11269-022-03156-7.

Abd-Elaty, I., Straface, S., Kuriqi, A., 2021. Sustainable saltwater intrusion management in coastal aquifers under climatic changes for humid and hyper-arid regions. Ecol. Eng. 171, 106382. http://dx.doi.org/10.1016/j.ecoleng.2021.106382.

Abdoulhalik, A., Abdelgawad, A.M., Ahmed, A.A., Moutari, S., Hamill, G., 2022. Assessing the protective effect of cutoff walls on groundwater pumping against saltwater upconing in coastal aquifers. J. Environ. Manag. 323, 116200. http://dx.doi.org/10.1016/j.jenvman.2022.116200.

Abdoulhalik, A., Ahmed, A.A., 2017. How does layered heterogeneity affect the ability of subsurface dams to clean up coastal aquifers contaminated with seawater intrusion? J. Hydrol. 553, 708–721. http://dx.doi.org/10.1016/j.jhydrol.2017.08.044.

Abdoulhalik, A., Ahmed, A., Hamill, G.A., 2017. A new physical barrier system for seawater intrusion control. J. Hydrol. 549, 416–427. http://dx.doi.org/10.1016/j.jhydrol.2017.04.005.

Al-Yaqoubi, S., Al-Maktoumi, A., Kacimov, A., Abdalla, O., Al-Belushi, M., 2021. Fresh-saline water dynamics in coastal aquifers: Sand tank experiments with mar-wells injecting at intermittent regimes. J. Hydrol. 601, 126826. http://dx.doi.org/10.1016/j.jhydrol.2021.126826.

Armanuos, A.M., Al-Ansari, N., Yaseen, Z.M., 2020. Underground barrier wall evaluation for controlling saltwater intrusion in sloping unconfined coastal aquifers. Water 12 (9), 2403. http://dx.doi.org/10.3390/w12092403.

Armanuos, A.M., Ibrahim, M.G., Mahmod, W.E., Takemura, J., Yoshimura, C., 2019. Analysing the combined effect of barrier wall and freshwater injection countermeasures on controlling saltwater intrusion in unconfined coastal aquifer systems. Water Resour. Manag. 33 (4), 1265–1280. http://dx.doi.org/10.1007/s11269-019-2184-9.

Carretero, S., Rapaglia, J., Bokuniewicz, H., Kruse, E., 2013. Impact of sea-level rise on saltwater intrusion length into the coastal aquifer, Partido de La Costa, Argentina. Cont. Shelf Res. 61–62, 62–70. http://dx.doi.org/10.1016/j.csr.2013.04.029.

Chang, S.W., Clement, T.P., Simpson, M.J., Lee, K.-K., 2011. Does sea-level rise have an impact on saltwater intrusion? Adv. Water Resour. 34 (10), 1283–1291. http://dx.doi.org/10.1016/j.advwatres.2011.06.006.

Chang, Q., Zheng, T., Chen, Y., Zheng, X., Walther, M., 2020. Investigation of the elevation of saltwater wedge due to subsurface dams. Hydrol. Process. 34 (22), 4251–4261. http://dx.doi.org/10.1002/hyp.13863.

Chang, Q., Zheng, T., Chen, Y., Zheng, X., Walther, M., 2021. Influence of inland freshwater influx on the natural desalination of coastal aquifers with a cutoff wall. Desalination 499, 114863. http://dx.doi.org/10.1016/j.desal.2020.114863.

Chang, Q., Zheng, T., Zheng, X., Gao, C., Song, X., Walther, M., 2023. Repulsion driven by groundwater level difference around cutoff walls on seawater intrusion in unconfined aquifers. Sci. Total Environ. 874, 162535. http://dx.doi.org/10.1016/j.scitotenv.2023.162535.

Chang, Q., Zheng, T., Zheng, X., Zhang, B., Sun, Q., Walther, M., 2019. Effect of subsurface dams on saltwater intrusion and fresh groundwater discharge. J. Hydrol. 576, 508–519. http://dx.doi.org/10.1016/j.jhydrol.2019.06.060.

Cosby, A.G., Lebakula, V., Smith, C.N., Wanik, D.W., Bergene, K., Rose, A.N., Swanson, D., Bloom, D.E., 2024. Accelerating growth of human coastal populations at the global and continent levels: 2000–2018. Sci. Rep. 14 (1), http://dx.doi.org/10.1038/s41598-024-73287-x.

Fang, Y., Qian, J., Zheng, T., Wang, H., Zheng, X., Walther, M., 2023. Submarine groundwater discharge in response to the construction of subsurface physical barriers in coastal aquifers. J. Hydrol. 617, 129010. http://dx.doi.org/10.1016/j.jhydrol.2022.129010.

Gao, M., Zheng, T., Chang, Q., Zheng, X., Walther, M., 2021. Effects of mixed physical barrier on residual saltwater removal and groundwater discharge in coastal aquifers. Hydrol. Process. 35 (7), http://dx.doi.org/10.1002/hyp.14263.

Green, T.R., Taniguchi, M., Kooi, H., Gurdak, J.J., Allen, D.M., Hiscock, K.M., Treidel, H., Aureli, A., 2011. Beneath the surface of global change: Impacts of climate change on groundwater. J. Hydrol. 405 (3–4), 532–560. http://dx.doi.org/10.1016/j.jhydrol.2011.05.002.

Ishida, S., Tsuchihara, T., Yoshimoto, S., Imaizumi, M., 2011. Sustainable use of groundwater with underground dams. Jpn. Agric. Res. Q.: JARQ 45 (1), 51–61. http://dx.doi.org/10.6090/jarq.45.51.

Kacimov, A.R., Sherif, M.M., Perret, J.S., Al-Mushikhi, A., 2009. Control of sea water intrusion by saltwater pumping: Coast of Oman. Hydrogeol. J. 17 (3), 541–558. http://dx.doi.org/10.1007/s10040-008-0425-8.

Kaleris, V.K., Ziogas, A.I., 2013. The effect of cutoff walls on saltwater intrusion and groundwater extraction in coastal aquifers. J. Hydrol. 476, 370–383. http://dx.doi.org/10.1016/j.jhydrol.2012.11.007.

Konikow, L.F., 2011. Contribution of global groundwater depletion since 1900 to sea-level rise. Geophys. Res. Lett. 38 (17), http://dx.doi.org/10.1029/2011GL048604.

Langevin, C.D., Thorne, D.T., Dausman, A.M., Sukop, M.C., Guo, W., 2008. SEAWAT Version 4: A Computer Program for Simulation of Multi-Species Solute and Heat Transport. In: USGS Numbered Series Techniques and Methods 6-A22, US Geological Survey, p. vi, 39 p.

Lu, C., Werner, A.D., 2013. Time-scales of seawater intrusion and retreat. Adv. Water Resour. 59, 39–51. http://dx.doi.org/10.1016/j.advwatres.2013.05.005.

Luyun, R., Momii, K., Nakagawa, K., 2009. Laboratory-scale saltwater behavior due to subsurface cutoff wall. J. Hydrol. 377 (3–4), 227–236. http://dx.doi.org/10.1016/j.jhydrol.2009.08.019.

Luyun, R., Momii, K., Nakagawa, K., 2011. Effects of recharge wells and flow barriers on seawater intrusion. Groundwater 49 (2), 239–249. http://dx.doi.org/10.1111/j.1745-6584.2010.00719.x.

Miao, T., Lu, W., Lin, J., Guo, J., Fan, Y., 2019. Simulation of seawater intrusion and optimization of cutoff wall schemes based on surrogate model. Hum. Ecol. Risk Assess.: Int. J. 25 (1–2), 297–313. http://dx.doi.org/10.1080/10807039.2018.1553611.

Moe, H., Hossain, R., Fitzgerald, R., Banna, M., Mushtaha, A., Yaqubi, A., 2001. Application of a 3-dimensional coupled flow and transport model in the Gaza Strip. In: Proceedings of the First International Conference and Workshop on Saltwater Intrusion and Coastal Aquifers: Monitoring, Modeling, and Management (SWICA-M3).

Morgan, L.K., 2024. Sea-level rise impacts on groundwater: exploring some misconceptions with simple analytic solutions. Hydrogeol. J. 32 (5), 1287–1294. http://dx.doi.org/10.1007/s10040-024-02791-1.

Morgan, L.K., Bakker, M., Werner, A.D., 2015. Occurrence of seawater intrusion overshoot. Water Resour. Res. 51 (4), 1989–1999. http://dx.doi.org/10.1002/2014WR016329.

Morgan, L.K., Stoeckl, L., Werner, A.D., Post, V.E.A., 2013. An assessment of seawater intrusion overshoot using physical and numerical modeling. Water Resour. Res. 49 (10), 6522–6526. http://dx.doi.org/10.1002/wrcr.20526.

Motallebian, M., Ahmadi, H., Raoof, A., Cartwright, N., 2019. An alternative approach to control saltwater intrusion in coastal aquifers using a freshwater surface recharge canal. J. Contam. Hydrol. 222, 56–64. http://dx.doi.org/10.1016/j.jconhyd.2019.02.007.

Nam, B., Solórzano-Rivas, C., Jazayeri, A., Werner, A.D., 2025. Tidal, freshwater-saltwater interactions: Three-dimensional sand-tank experiments. J. Hydrol. 653, 132696. http://dx.doi.org/10.1016/j.jhydrol.2025.132696, ISSN 0022-1694.

Nishigaki, M., Kankam-Yeboah, K., Komatsu, M., 2004. Underground dam technology in some parts of the world. J. Groundw. Hydrol. 46 (2), 113–130. http://dx.doi.org/10.5917/jagh1987.46.113.

Pool, M., Carrera, J., 2009. Dynamics of negative hydraulic barriers to prevent seawater intrusion. Hydrogeol. J. 18 (1), 95–105. http://dx.doi.org/10.1007/s10040-009-0516-1.

Reimann, L., Vafeidis, A.T., Honsel, L.E., 2023. Population development as a driver of coastal risk: Current trends and future pathways. Camb. Prism.: Coast. Future 1, http://dx.doi.org/10.1017/cft.2023.3.

Sadhasivam, R., Srinivasan, V., Clement, T.P., 2025. Hydrological implications of inland boundary conditions in coastal aquifers subject to sea level rise. Hydrogeol. J. 33 (7), 1877–1895. http://dx.doi.org/10.1007/s10040-025-02974-4.

Scanlon, B.R., Jolly, I., Sophocleous, M., Zhang, L., 2007. Global impacts of conversions from natural to agricultural ecosystems on water resources: Quantity versus quality. Water Resour. Res. 43 (3), http://dx.doi.org/10.1029/2006WR005486.

Shen, Y., Xin, P., Yu, X., 2020. Combined effect of cutoff wall and tides on groundwater flow and salinity distribution in coastal unconfined aquifers. J. Hydrol. 581, 124444. http://dx.doi.org/10.1016/j.jhydrol.2019.124444.

Sherif, M.M., Singh, V.P., 1999. Effect of climate change on sea water intrusion in coastal aquifers. Hydrol. Process. 13 (8), 1277–1287. http://dx.doi.org/10.1002/(SICI)1099-1085(19990615)13:8<1277::AID-HYP765>3.0.CO;2-W.

Sun, D.-m., Niu, S.-x., Zang, Y.-g., 2017. Impacts of inland boundary conditions on modeling seawater intrusion in coastal aquifers due to sea-level rise. Nat. Hazards 88 (1), 145–163. http://dx.doi.org/10.1007/s11069-017-2860-0.

Talbot, L.E.D., Given, J., Tjung, E.Y.S., Liang, Y., Chowdhury, K., Seed, R., Soga, K., 2024. Modeling large-deformation features of the Lower San Fernando dam failure with the Material Point Method. Comput. Geotech. 165, 105881. http://dx.doi.org/10.1016/j.compgeo.2023.105881.

Taylor, R.G., Scanlon, B., Döll, P., Rodell, M., Beek, R.van., Wada, Y., Longuevergne, L., Leblanc, M., Famiglietti, J.S., Edmunds, M., Konikow, L., Green, T.R., Chen, J., Taniguchi, M., Bierkens, M.F.P., MacDonald, A., Fan, Y., Maxwell, R.M., Yechieli, Y., Gurdak, J.J., Allen, D.M., Shamsudduha, M., Hiscock, K., Yeh, P.J.-F., Holman, I., Treidel, H., 2012. Ground water and climate change. Nat. Clim. Chang. 3 (4), 322–329. http://dx.doi.org/10.1038/nclimate1744.

Voldoire, A., Sanchez-Gomez, E., Mélia, D.Salas.y., Decharme, B., Cassou, C., Sénési, S., Valcke, S., Beau, I., Alias, A., Chevallier, M., Déqué, M., Deshayes, J., Douville, H., Fernandez, E., Madec, G., Maisonnave, E., Moine, M.-P., Planton, S., Saint-Martin, D., Szopa, S., Tyteca, S., Alkama, R., Belamari, S., Braun, A., Coquart, L., Chauvin, F., 2013. The CNRM-CM5.1 global climate model: Description and basic evaluation. Clim. Dyn. 40 (9–10), 2091–2121. http://dx.doi.org/10.1007/s00382-011-1259-y.

Wada, Y., van Beek, L.P.H., van Kempen, C.M., Reckman, J.W.T.M., Vasak, S., Bierkens, M.F.P., 2010. Global depletion of groundwater resources. Geophys. Res. Lett. 37 (20), http://dx.doi.org/10.1029/2010GL044571.

Werner, A.D., Bakker, M., Post, V.E.A., Vandenbohede, A., Lu, C., Ataie-Ashtiani, B., Simmons, C.T., Barry, D.A., 2013. Seawater intrusion processes, investigation and management: Recent advances and future challenges. Adv. Water Resour. 51, 3–26. http://dx.doi.org/10.1016/j.advwatres.2012.03.004.

Wu, H., Lu, C., Shen, C., Ye, Y., 2023. Using a subsurface barrier to control seawater intrusion and enhance groundwater extraction in coastal aquifers: An analytical study. J. Hydrol. 621, 129537. http://dx.doi.org/10.1016/j.jhydrol.2023.129537.

Zheng, T., Gao, M., Chang, Q., Zheng, X., Walther, M., 2022. Dynamic desalination of intruding seawater after construction of cutoff walls in a coastal unconfined aquifer. Front. Mar. Sci. 9, http://dx.doi.org/10.3389/fmars.2022.857807.

Zheng, T., Zheng, X., Chang, Q., Zhan, H., Walther, M., 2021. Time-scale and effectiveness of residual saltwater desalinization behind subsurface dams in an unconfined aquifer. Water Resour. Res. 57 (2), http://dx.doi.org/10.1029/2020WR028493.

Zheng, T., Zheng, X., Sun, Q., Wang, L., Walther, M., 2020. Insights of variable permeability full-section wall for enhanced control of seawater intrusion and nitrate contamination in unconfined aquifers. J. Hydrol. 586, 124831. http://dx.doi.org/10.1016/j.jhydrol.2020.124831.